High-strong-ductile magnesium alloys by interactions of nanoscale quasi-long period stacking order unit with twin.

ZHOU, L., NIU, T., ZOU, G., SU, H., HE, S., ZHENG, S., ZHU, Y., CHEN, P., FERNANDEZ, C. and PENG, Q.

2024

Available online at www.sciencedirect.com
ScienceDirect
Journal of Magnesium and Alloys xxx (xxxx) xxx
www.elsevier.com/locate/jma

Full Length Article

High-strong-ductile magnesium alloys by interactions of nanoscale quasi-long period stacking order unit with twin

Lutong Zhou[a], Tingting Niu[a], Guodong Zou[a,*], Huhu Su[b], Suyun He[b], Shijian Zheng[b], Yulong Zhu[c], Peng Chen[c], Carlos Fernandez[d], Qiuming Peng[a,*]

[a] State Key Laboratory of Metastable Materials Science and Technology, Yanshan University, Qinhuangdao, 066004, PR China
[b] School of Materials Science and Engineering, Hebei University of Technology, Tianjin, 300401, PR China
[c] Key Laboratory of Automobile Materials of Ministry of Education & School of Materials Science and Engineering, Nanling Campus, Jilin University, Changchun 130025, PR China
[d] School of Pharmacy and life sciences, Robert Gordon University, Aberdeen, AB107GJ, UK

Received 18 October 2023; received in revised form 1 December 2023; accepted 7 January 2024
Available online xxx

Abstract

Magnesium alloys with high strength in combination of good ductility are especially desirable for applications in transportation, aerospace and bio-implants owing to their high stiffness, abundant raw materials, and environmental friendliness. However, the majority of traditional strengthening approaches including grain refining and precipitate strengthening can usually prohibit dislocation movement at the expense of ductility invariably. Herein, we report an effective strategy for simultaneously enhancing yield strength (205 MPa, 2.41 times) and elongation (23%, 1.54 times) in a Mg-0.2Zn-0.6Y (at.%) alloy at room temperature, based on the formation of a nanosized quasi-long period stacking order unit (QLPSO)-twin structure by ultrahigh-pressure treatment followed by annealing. The formation reason and strong-ductile mechanism of the unique QLPSO-twin structure have been clarified by transmission electron microscopy observations and molecule dynamics simulations. The improved strength is mainly associated with the presence of nanosized QLPSO and the modified ∠86.3° QLPSO-twin boundary (TB) interface, effectively pinning dislocation movement. Comparatively, the enhanced ductility is related to the ∠3.7° QLPSO-TB interface and micro-kinks of nanoscale QLPSO, providing some paths for plastic deformation. This strategy on the QLPSO-twin structure might provide an alternative perspective for designing innovative hexagonal close-packed structural materials with superior mechanical properties.

Keywords: QLPSO; Twin boundary; Molecule dynamics; High resolution TEM.

1. Introduction

The development of high strength-ductility Mg alloys has received considerable attention for applications due to the increasing demands of lightweight materials for energy-efficiency and green environment, and then attributes to the achievement of dual-carbon target. Although they possess high specific strength and good cast-ability, there are, however, two bottlenecks relative to low strength and limited ductility at room temperature severely impede their widespread applications as potential structural materials [1]. Consequently, a large number of methods in the past decades relative to alloying, grain refining, composites and texture engineering, have been extensively performed to improve their mechanical properties [2–4]. Essentially, these methods dependent on incoherent interfaces, such as grain boundaries and metastable phases, can effectively prohibit dislocation movement, whereas they also significantly reduce the ductility. In this regard, improving strength and ductility of Mg alloys

* Corresponding authors.
E-mail addresses: zouguodong@ysu.edu.cn (G. Zou), pengqiuming@ysu.edu.cn (Q. Peng).

https://doi.org/10.1016/j.jma.2024.01.015

Please cite this article as: L. Zhou, T. Niu, G. Zou et al., High-strong-ductile magnesium alloys by interactions of nanoscale quasi-long period stacking order unit with twin, Journal of Magnesium and Alloys, https://doi.org/10.1016/j.jma.2024.01.015

simultaneously is of significant importance but a grand challenge so far.

Contrary to incoherent boundaries, coherent twin boundaries bestow high strength in combination with good ductility. For instance, twins can provide a coherent internal interface in ultrafine-grained face-centered-cubic (FCC) copper [5], offering outstanding mechanical properties, especially at the nanoscale level. Additionally, the ultrahard cubic boron nitride [6] and nano-twinned diamond composites have continuously exceeded the hardness margin, with toughness comparable to that of Al alloys [7]. Inspired by twin strengthening in FCC metals and ceramics, twin interface modifications in HCP metals might be anticipated to attain high strength together with good ductility. Unfortunately, two difficulties should be solved before introducing this pathway. On the one hand, the volume fraction of twin boundaries is limited. The most common twin mode in Mg alloys is $\{10\bar{1}2\}$ tension twins (TTWs). However, the interface of TTWs is unstable, and then it is ready to widen rather than proliferate [8]. On the other hand, the critical resolved shear stress (CRSS) value of perfect TTW is merely ~10 MPa [9]. In this case, twin boundaries modification play a crucial role in plastic deformation, and thereby determining formability and mechanical properties of HCP-type Mg alloys. More recently, we have achieved two new coherent twin interfaces: the hierarchical $\{10\bar{1}1\}$-$\{10\bar{1}1\}$ double contraction twins [10] and the $\{10\bar{1}1\}$ contraction twins-stacking faults [11], by an industrial ultrahigh pressure (UP) technique in Mg-Li alloys. These structures can remarkably improve microhardness and yield strength without sacrificing the ductility at room temperature, demonstrating that the modification of twin interfaces is a possible route to realize good mechanical properties.

In addition, the long period stacking order (LPSO) phase is another partial coherent component to improve the mechanical properties of Mg alloys. Specifically, the *a* spacing value of 18R-type LPSO is 0.351 nm [12], which is the same as that of Mg matrix, suggesting it is fully coherent along the basal direction to accommodate strain. Comparatively, the *c* spacing of 18R-type LPSO (four-layered atoms) is 0.798 nm, nearly corresponding Mg matrix (four-layered atoms, 0.781 nm) [13,14]. It reveals that it can not only pin dislocation motion with a lattice mismatch of 1.2 %, but also coordinate its deformation under high strain conditions. The main shortage for LPSO phase strengthening is related to large dimension of lamellar LPSO, and it severely prohibits the nucleation and growth of twins, resulting in high strength but low contribution in ductility [15].

Provided that we can reduce the thickness of the LPSO phase to one ideal unit (four-layered atoms), this structure, analogous to the Y/Zn atoms preferentially segregate at stacking faults, can effectively prohibit dislocation movement. Simultaneously, it is prone to form deformation twin, resulting in the increment of coherent interface fraction. More importantly, the one-united LPSO phase, similar to deformed stacking faults, will contact twin boundaries (TBs) and remarkably improve the CRSS of TB slipping. Therefore, the structure might enhance both strength and ductility by providing effective dislocation pinning sites together with possible interface deformation modes. Herein, we report a unique structure-nanosized quasi-long period stacking order unit (QLPSO)-twin structure in a low alloying Mg-0.2Zn-0.6Y (at.%) sample (the normal matrix composition of as-cast $Mg_{97}Zn_1Y_2$ alloy) by ultrahigh pressure (UP) followed by annealing. The atomic microstructure, two interactive roles between QLPSO and twin, and strong-ductile mechanism of this distinctive structure are investigated by high-resolution transmission electron microscopy (HRTEM) and molecular dynamics (MD) simulations.

2. Experimental procedure

2.1. Sample preparation

The alloy with a nominal composition of Mg-0.2Zn-0.6Y (at.%) alloy was utilized to carry out the experiments. The cast bar with a diameter of 120 mm was prepared by high pure raw materials in an electromagnetic induction melting furnace using a graphite crucible under the protection of SF6 atmosphere. The chemical composition of the as-cast sample was analyzed by inductively coupled plasma atomic emission spectroscopy (ICP-AES). The main elemental compositions (at.%) were Zn (0.16), Y (0.54) and the balance of Mg. The total impurity concentration is below 0.1 at. %.

The cast bar was machined into cylindrical specimens with a diameter of 60 mm and a length of 15 mm for UPed treatment in an industrial CS-IB type hexahedral anvil apparatus. First, the sample was wrapped with tantalum foil and inserted in a BN capsule which was thermally stable. And then, the samples were heated in a graphite furnace, and a cubic pyrophyllite filled the role of the pressure medium. The hydrostatic pressure could be obtained by the press along three axes. The samples were treated in a temperature range of 500 to 1100°C under a pressure of 4 GPa. The holding time was 30 min. Theoretically, Clausius-Clapeyron equation shows the relationship between the slope of the temperature pressure change of the phase and the molar latent heat and the changed volume of the phase transition. Since the volume of magnesium alloy expands and the molar latent heat is positive during melting, the slope of temperature and pressure change is positive. Therefore, heat treatment beyond the melting point of magnesium alloys under high pressure is possible. Experimentally, this phenomenon that the melting point of the alloy increases under high pressure conditions has been confirmed in our previous articles [10,11]. Finally, the samples were quenched to room temperature directly before unloading pressure. After UPed treatment, the UPed samples have been annealed for 1 h under argon gas at different temperatures. Noticeably, the UPed sample under 4 GPa at 800 °C heat-treated at 300 °C was denoted as UPed800-A300. The as-cast (AC) and as-UPed800 samples were involved as references.

2.2. Mechanical properties

Hardness was measured in a FM-ARS-9000 Vickers hardness tester. The test load and loading times are 200 g and 10 s,

Please cite this article as: L. Zhou, T. Niu, G. Zou et al., High-strong-ductile magnesium alloys by interactions of nanoscale quasi-long period stacking order unit with twin, Journal of Magnesium and Alloys, https://doi.org/10.1016/j.jma.2024.01.015

respectively. The average hardness value has been calculated in terms of 5 × 5 matrix measures. Mechanical tests were performed on the INSTRON 5848 MicroTester at a strain rate of 1×10^{-3} s^{-1}. The dog bone-shaped tensile samples had a gauge length of 20 mm, a width of 2 mm and a thickness of 1.5 mm. At least five parallel samples were tested to obtain the average values. The value was averaged over at least three measurements

2.3. Microstructural characterization

The microstructural investigations were performed using an optical microscopy (OM) and scanning electron microscopy (SEM). Samples for OM and SEM were prepared by a procedure involving grinding up to 2400 SiC paper, followed by mechanical polishing with 9, 3 and 1 μm water-free diamond suspensions and finally polished using 0.05 μm colloidal silica. The final step included chemical polishing in a fresh solution containing a mixture of 100 mL of methanol, 12 mL of hydrochloric acid, and 8 mL of nitric acid. The grain size was calculated by Image Pro Plus software. Multiple OM images were selected for each state of the sample for statistics and averaging. It is difficult to calculate the grain size of the as-cast samples with dendrite morphology. We shoot the samples by polarizing light mounted on the optical microscope, and distinguish the grain boundary by different color contrast, and then calculate the grain size artificially.

The microstructure of the deformation characters was mainly characterized by Talos-F200 transmission electron microscope (TEM) and JEM-ARM300F aberration-corrected scanning TEM (STEM) operated at a voltage of 300 kV. Specimens for TEM observation were extracted from the deformed samples (~5 %) and thinned using mechanical grinding to 30 μm. Then, the specimens were prepared by low energy (3.5 keV) ion-milling (PIPS II System). Finally, all TEM samples were cleaned by Solarus II Plasma Cleaner.

2.4. MD simulations

To reveal the interaction mechanism between the QLPSO phase and $\{10\bar{1}2\}$ twinning, molecular dynamics (MD) simulations were performed using the large-scale atomic/molecular massively parallel simulator (LAMMPS) [16]. The interatomic potential of the Mg-Zn-Y ternary system was not available in the literature because developing a reliable one was highly challenging. Therefore, we used a hybrid atomic potential which was a combination of Lennard–Jones (L–J) potential with Modified Embedded-Atom Method (MEAM) potential [17]. Specifically, MEAM potentials developed by Lee al [18,19]. were used to describe the interaction for Mg-Mg, Mg-Zn, Mg-Y, Zn-Zn, and Y-Y pairs, and a L-J potential was adopted to describe the interaction of the Y-Zn pair. The L-J potential was shown in the following form,

$$E = 4\epsilon\left[\left(\frac{\sigma}{r}\right)^{12} - \left(\frac{\sigma}{r}\right)^{6}\right], \quad r < r_c \tag{1}$$

where ε, σ and r_c were the well-depth, distance parameter diameter, and cutoff radius of the potential. The parameters ε and σ for Y-Zn pairs were obtained following the Lorentz-Berthelot mixing rule [20],

$$\varepsilon_{Y-Zn} = \sqrt{\varepsilon_Y \varepsilon_{Zn}} \tag{2}$$

$$\sigma_{Y-Zn} = \frac{\sigma_Y + \sigma_{Zn}}{2} \tag{3}$$

where $\varepsilon_{Zn} \approx 0.00538$ eV, $\sigma_{Zn} \approx 2.46$ Å, $\varepsilon_Y \approx 0.00312$ eV, $\sigma_Y \approx 2.98$ Å [21]. Thus, the ε_{Y-Zn} and σ_{Y-Zn} were 0.00408 eV and 2.70 Å, respectively.

To set up the simulation system, a bicrystal was first constructed to satisfy the perfect $\{10\bar{1}2\}\langle 10\bar{1}\bar{1}\rangle$ twin relationship. Then, the QLPSO or LPSO was pre-planted in the parent lattice. Dimensions of all simulation models with QLPSO and LPSO structures were approximately $23 \times 36 \times 26$ nm^3, containing ~900 000 atoms. No periodic boundary condition was applied. The conjugate gradient algorithm was used to perform energy minimization followed by further relaxation at 100 K within the microcanonical (NVE) ensemble for 20 ps. A simple shear strain was applied to cause TB to migrate and then interacted with the QLPSO. The stain rate was $\sim 10^{10}$ /s, and the time-step was 1.0 fs. The visualization software Ovito was used to analyze and visualize the simulation results.

Movie S1. Comparison of the interactions between QLPSO with different layers and twins.
Movie S2. The formation of ∠3.7° QLPSO-twin structure.
Movie S3. Structure transformation process from ∠86.3° QLPSO-twin to ∠ 3.7° QLPSO-twin.

3. Results

3.1. Mechanical properties

Fig. 1a shows the hardness variation of UPed Mg-0.2Zn-0.6Y samples treated under different conditions. Specifically, the hardness values show two typical characteristics. On the one hand, a presentative "V-shaped" trend is detected under a constant pressure of 4 GPa during the whole temperature range. The value of the as-cast sample is about 62±2 HV, which is remarkably reduced with increasing UPed temperature. The lowest value of 56±2 HV is attained for the UPed800 sample. Subsequently, the values are increased with further increasing the UPed temperature. According to the optical observations (Fig. 1a), a typical UPed solid solution is confirmed in the range of 700-800 °C at 4 GPa, as evidenced by the elimination of dendrite structure in combination of the appearance of equiaxed grain. When the temperature is over 800 °C, some dot-like particles in relation to the $Mg_{24}Y_5$ or Y-rich phases are observed in the UPed Mg-0.2Zn-0.6Y alloys [15], and they account for the improvement of hardness, resulting in the formation of V-shaped trend. It is worth noting that a typical dendrite microstructure is re-observed when the temperature is 1100 °C, in which its dendrite spacing is clearly lower than that of the as-cast sample. It demonstrates

Please cite this article as: L. Zhou, T. Niu, G. Zou et al., High-strong-ductile magnesium alloys by interactions of nanoscale quasi-long period stacking order unit with twin, Journal of Magnesium and Alloys, https://doi.org/10.1016/j.jma.2024.01.015

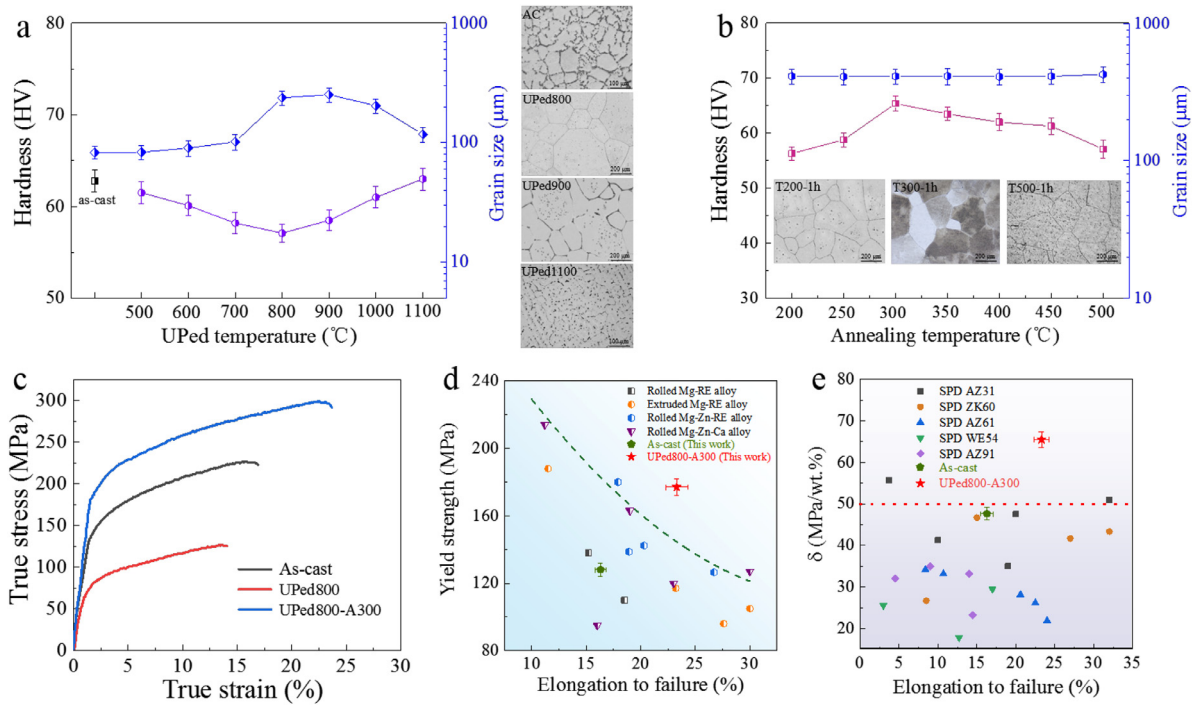

Fig. 1. Mechanical properties of Mg-0.2Zn-0.6Y alloys. (a) Hardness and grain size of different UPed samples. Typical optical structures of different samples. (b) Hardness and grain size of different annealed samples, the insets are optical structures. (c) Tensile curves of Mg-Zn-Y alloys prepared under different conditions. (d) Comparison of yield strength and elongation among low alloying Mg-RE and Mg-Zn-RE alloys by different fabrication techniques. (e) Comparison of strengthening role per atom of alloying element of commercial Mg alloys.

that the re-solidification process occurs during this process. Theoretically, the melting points of Mg-0.2Zn-0.6Y alloys increase as exterior pressure increases [22]. During the UPed solid solution treatment process, the synergistic role related to the decomposition/transformation of eutectic phases attributes to the V-shaped variation of hardness. To attain high volume fraction of strengthening phase, the UPed800 Mg-0.2Zn-0.6Y alloy has been annealed for different time intervals (Fig. 1b). The similar microstructure and grain size is remained, whereas a typical volcano-shaped trend is observed during the treatment process, wherein the peak hardness of 66±2 HV is achieved after annealing at 300 °C, which is the 1.17 and 1.07 times higher than those of UPed800 and as-cast Mg-0.2Zn-0.6Y specimens, respectively.

Fig. 1c shows the representative true stress-strain tensile curves of Mg-0.2Zn-0.6Y alloys at different states at room temperature. Compared with the as-cast and UPed800 Mg-0.2Zn-0.6Y alloys, both yield strength and ultimate tensile strength of the UPed800-A300 Mg-0.2Zn-0.6Y sample are improved remarkably. Specifically, the yield strength of UPed800-A300 Mg-0.2Zn-0.6Y sample is 205 MPa, respectively, which are 1.50 and 2.41 times higher than those of the as-cast and UPed800 Mg-0.2Zn-0.6Y alloys, respectively. More importantly, the elongation of the UPed800-A300 Mg-0.2Zn-0.6Y is simultaneously improved. The value is over 23 %, which is 1.31 and 1.54 times higher than those of the as-cast and UPed800 Mg-0.2Zn-0.6Y alloys, respectively. The unique phenomenon of simultaneously enhanced strength and elongation has hardly been reported in Mg alloys, which overwhelm those of severely-deformed Mg alloys with similar coarse grain dimension and composition, as summarized in Fig. 1d [23–27]. Attractively, it exhibits an outstanding strengthening efficiency (δ, yield strength per weight of alloying elements) of 67 MPa (Fig. 1e) [23,24,28–32], which is far higher than those of commercial deformed Mg alloys, signifying a promising application merit.

3.2. Nano-scaled QLPSO unit

As evidenced by TEM images (Fig. 2a), a typical period stacking order (LPSO) phase with a width of over 100 nm has been observed in the as-cast Mg-0.2Zn-0.6Y alloy. In the corresponding selected area electron diffraction (SAED) pattern of LPSO phase (Fig. 2b) with the incidence of electron beam direction of $[11\bar{2}0]_{Mg}$, some extra weaker spots are detected at positions n/6 (where n is an integer) between direct spot and $(0002)_{Mg}$ diffraction, indicating that the LPSO phase is 18R-type structure [13]. This is further confirmed by the atomic sequence lined as a …BABACBCBACAC… structure (Fig. 2c). A, B and C represent the different {0001} planes. The length along <0002> and $<10\bar{1}0>$ direction are 4.64 and 1.12 nm, respectively, which are fully consistent with that of the reported 18R phase in Mg-Zn-Y system [14].

Comparatively, there are a large number of nanoplates homogeneously distributed in the UPed800-A300 Mg-0.2Zn-0.6Y alloy (Fig. 2d). The SAED pattern shows that the nanoplates grow along the basal plane, and the crystallization relationship of nanoplates agrees well with that of 18R-

Please cite this article as: L. Zhou, T. Niu, G. Zou et al., High-strong-ductile magnesium alloys by interactions of nanoscale quasi-long period stacking order unit with twin, Journal of Magnesium and Alloys, https://doi.org/10.1016/j.jma.2024.01.015

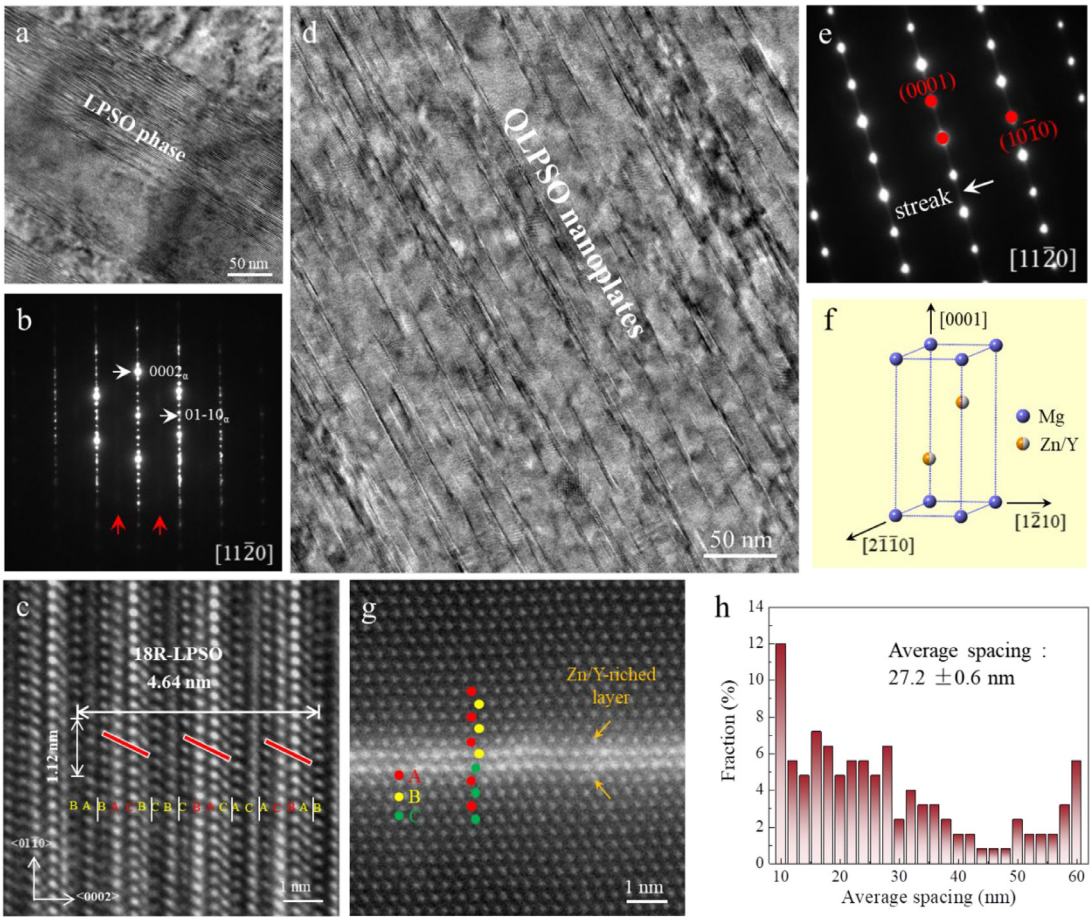

Fig. 2. Precipitation characteristics. Typical TEM image (a), SAED pattern (b) and atomic-level image (c) of the 18R-LPSO phase in the as-cast Mg-0.2Zn-0.6Y alloy. Bright field image (d), SAED pattern (e) and atomic-level HAADF image (g) of the QLPSO unit in UPed800-A300 Mg-0.2Zn-0.6Y alloy. (f) Schematic diagrams showing a unit cell of QLPSO phase. (h) The average spacing of QLPSO phase calculated based on 125 random dots.

LPSO (Fig. 2e), where the Zn/Y atoms occupy the Mg site, resulting in the formation of deformed hexagon closed packed structure. The layered nanoplate phase is mainly composed of four-layered atoms (Fig. 2f), and the medium layers become brighter owing to the replacement of heavy Zn or Y. The atom-arrange of nanoplate is a …ABABCACA… sequence, as proved in the high-resolution transmission electron microscopy (HRTEM) image (Fig. 2g). Therefore, this nanoplate-shaped phase can be denoted as a quasi-long period stacking order unit (QLPSO). The width of QLPSO is about 1 nm, and the average spacing distance is about 27.2 nm (Fig. 2h).

Nie et al. [33] reported the growth and transformation mechanism of LPSO phase. The growth of LPSO phase occurs by the generation and propagation of growth ledges. The development of these growth ledges involves the formation of building blocks with an ABCA-type stacking sequence, which are formed by the movement of Shockley partial dislocation with vector b=1/3<10$\bar{1}$0>. Additionally, the main feature of which is the significant enrichment and ordering of Y and Zn atoms within the B and C layers. In fact, an ideal QLPSO unit is part of the LPSO phase building block. Additionally, the main feature of the QLPSO phase is similar to LPSO phase. Therefore, we believe that the formation mechanism of QLPSO phase is the same as that of LPSO.

3.3. Hierarchical QLPSO-twin structures

The SEM image of UPed800-A300 Mg-0.2Zn-0.6Y alloy with a strain of 5 % (Fig. 3a) shows that some new oval-shaped twins with three different orientations are presented during the tension process, resulting in the formation of complex net-liked interactive structures with existed QLPSO phase. Specifically, two different hierarchical QLPSO-twin interactive structures have been identified by HRTEM observations. On the one hand, as exhibited in both TEM image and SAED pattern (Fig. 3b-c), it is clearly confirmed that the diffracted spots of $(0001)_M$ and $(0001)_T$ are rotates 86.3° to overlap in <11$\bar{2}$0> zone axes, suggesting the presentation of {10$\bar{1}$2} tension twins. Some steps with a height of two-layer atoms are also detected in the twin boundary of {10$\bar{1}$2} tension twins under HRTEM image (Fig. 4a,b). Therefore, it is deemed that the tension twin can nucleate and directly grow or slip through the matrix containing QLPSO phase as the

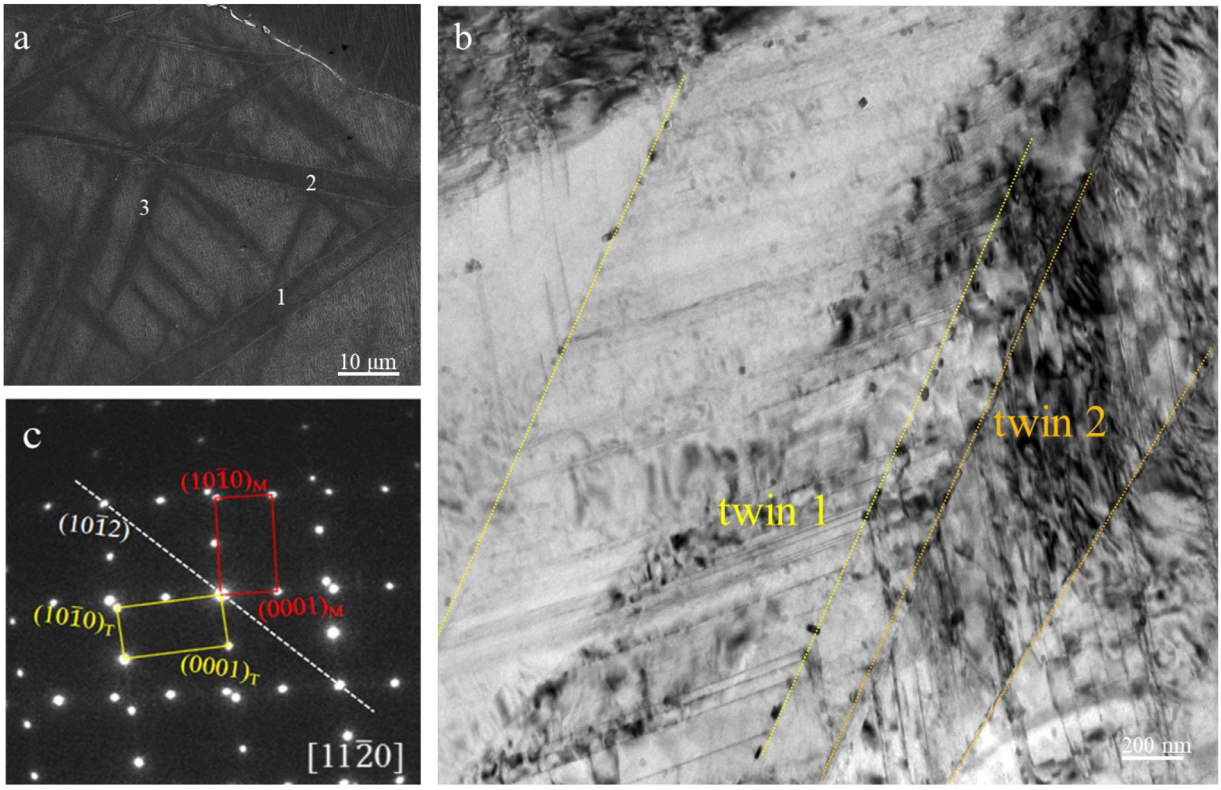

Fig. 3. Microstructure of the deformed UPed-A300 alloy ($\varepsilon = 5$ %). Local high resolution SEM image (a) and bright field image (b) of the deformed UPed-A300 Mg-0.2Zn-0.6Y alloy. (c) SAED pattern of twin interface along $[11\bar{2}0]$.

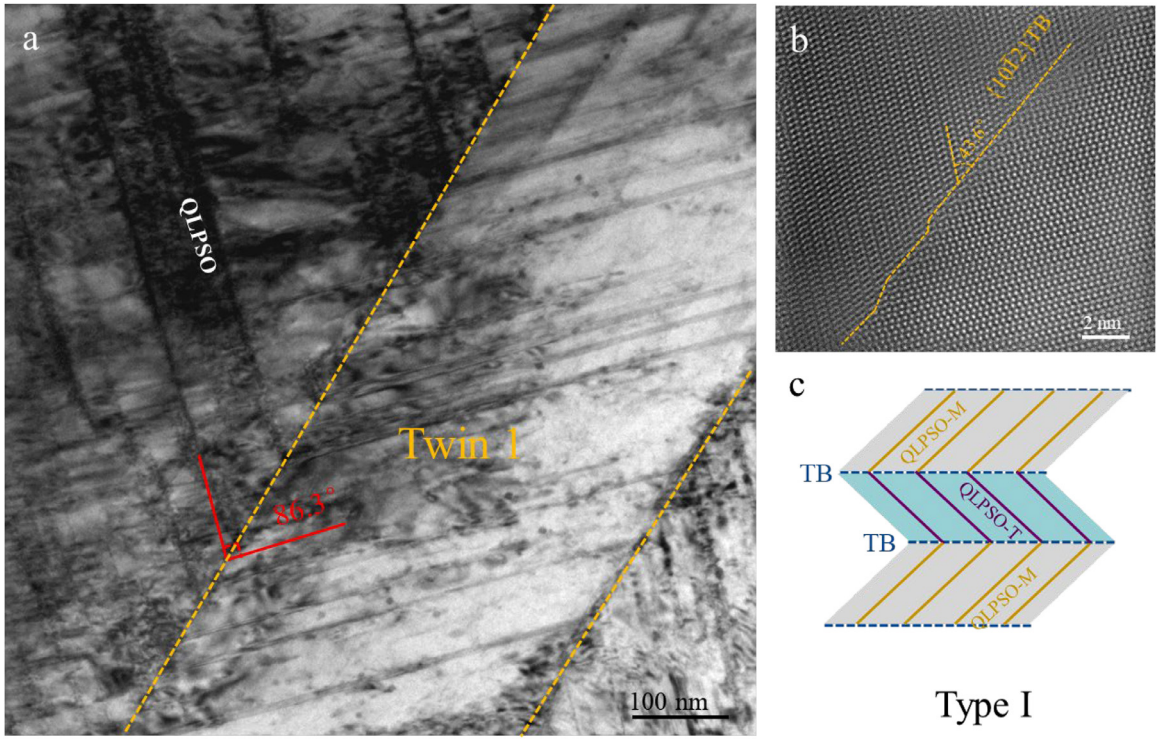

Fig. 4. Microstructural characteristic of the ∠86.3° QLPSO-twin structure in the deformed UPed800-A300 alloy ($\varepsilon = 5$ %). (a) Local high resolution images of the∠86.3° QLPSO phase (b) HRTEM image of tension twin boundary along $[11\bar{2}0]$. (c) Schematic of a hierarchical ∠86.3° QLPSO-twin structure.

Please cite this article as: L. Zhou, T. Niu, G. Zou et al., High-strong-ductile magnesium alloys by interactions of nanoscale quasi-long period stacking order unit with twin, Journal of Magnesium and Alloys, https://doi.org/10.1016/j.jma.2024.01.015

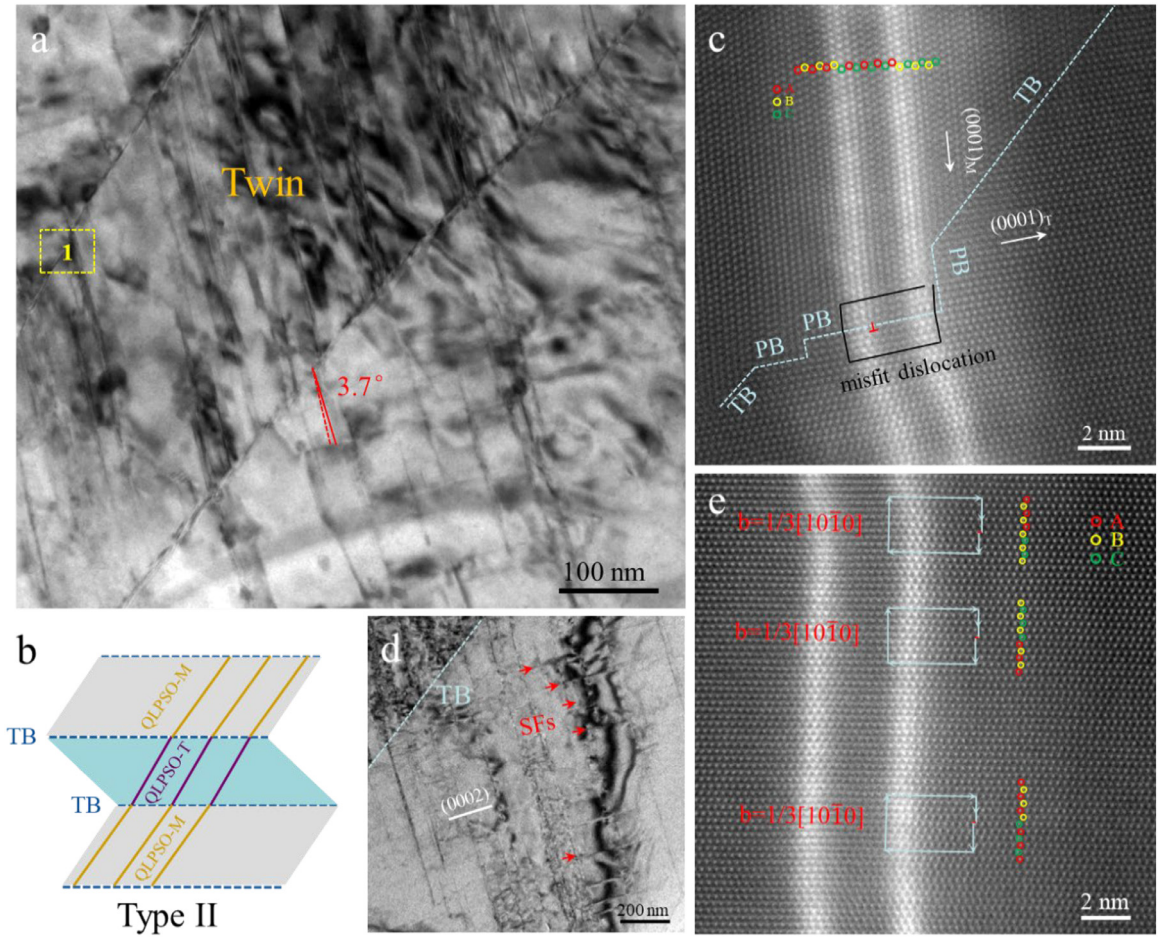

Fig. 5. Microstructural characteristic of the ∠3.7° QLPSO-twin structure in the deformed UPed800-A300 alloy (ε = 5 %). (a) Bright field TEM image of the structure. (b) Schematic of the ∠3.7° QLPSO-twin structure. (c) Atomic-resolution HAADF-STEM image taken from region I, indicated in (a). (d) Bright field image of the structure interior the {10$\bar{1}$2} twin. (e) Atomic-resolution HAADF-STEM image of the interaction between QLPSO phase and basal SFs.

strain is increasing. Subsequently, the QLPSO phase is completely retorted along the basal plane of twin, resulting in the formation of 86.3° reversion (Type-I, Fig. 4c).

On the other hand, there exists another interactive interface reaction between {10$\bar{1}$2} tension twin and QLSPO phase. Fig. 5a shows that the twin boundary almost straightly cuts through QLPOS phase, merely with a retorted angle of 3.7°, resulting in the formation of hierarchical ∠3.7° QLPSO-twin structure (Type II, Fig. 5b). Noticeably, a typical strain band in twin boundary is observed, and the twin boundary in the hierarchical ∠3.7° QLPSO-twin structure becomes wider in contrast to that in the hierarchical ∠86.3° QLPSO-twin structure. Moreover, under HRTEM image (Fig. 5c), the typical terraced boundaries consisting of co-existing PB interfaces and twin boundary are observed, indicating that twin boundary and PB interface can transform to each other during the boundary migration process [34]. In addition, a large number of basal stacking faults (SFs) are detected in the interior of QLPSO (Fig. 5d), and they are vertical to the QLPSO orientation. The atomic-resolution HAADF-STEM image (Fig. 5e) reveals that the SFs were assigned to a growth fault (I_1-type), which is formed by removing an A plane above a B plane, and then shearing the remaining planes above the B plane by 1/3[10$\bar{1}$0], resulting in a …ABABABCBCBCB… structure [35]. Evidently, this homogenously distributed QLPSO phase with a nanoscale dimension hardly affects the deformation mode, especially at low temperatures. Namely, the existence of QLPSO phase can not prohibit the appearance of tension twins, which is different from the twin-inhibition behavior of bulked LPSO phase [15].

4. Discussion

4.1. The formation of QLPSO-twin structure

The unique QLPSO-twin structure has been identified during the plastic deformation (5 % strain) in the UPed800-A300 Mg-0.2Zn-0.6Y alloy, which accounts for its high strength together with outstanding elongation. The formation of this unique structure has been elucidated by MD simulations. It has been recognized that LPSO phases have long period stacking order with a local stacking sequence different from the matrix and exhibit chemical order with segregation of solute atoms. In this work, the 18R-LPSO structures are con-

Please cite this article as: L. Zhou, T. Niu, G. Zou et al., High-strong-ductile magnesium alloys by interactions of nanoscale quasi-long period stacking order unit with twin, Journal of Magnesium and Alloys, https://doi.org/10.1016/j.jma.2024.01.015

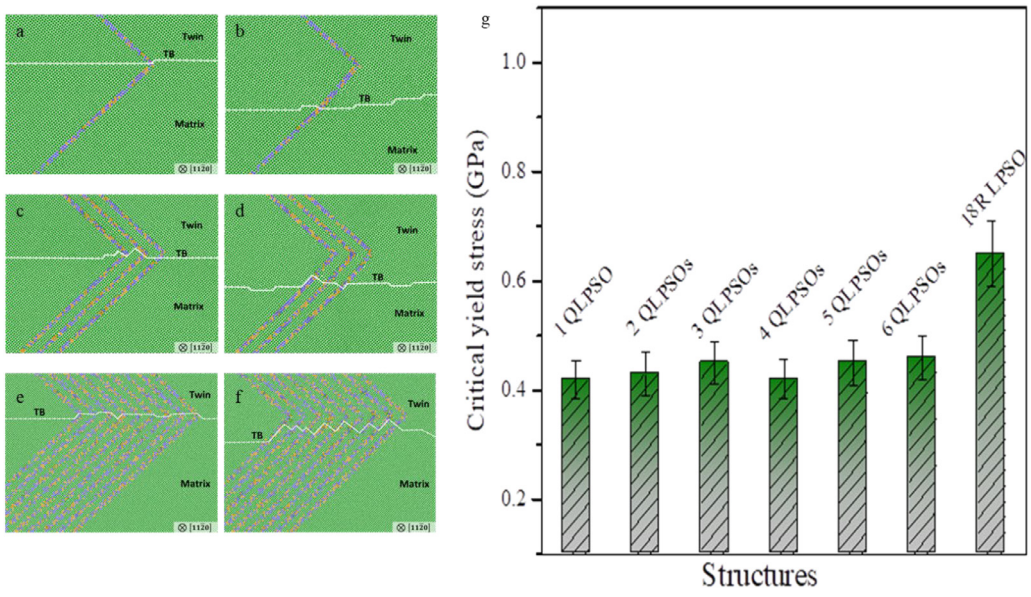

Fig. 6. MD simulations of the interactive roles between QLPSO and $\{10\bar{1}2\}$ twin. The prohibition role of the different numbers of QLPSO layers on twin boundary movement (captured from Movie 1), (a,b) single QLPSO, (c,d) three QLPSOs, (e,f) 18R LPSO. (g) Comparison of critical yield stress of different structures between QLPSOs and 18R LPSO.

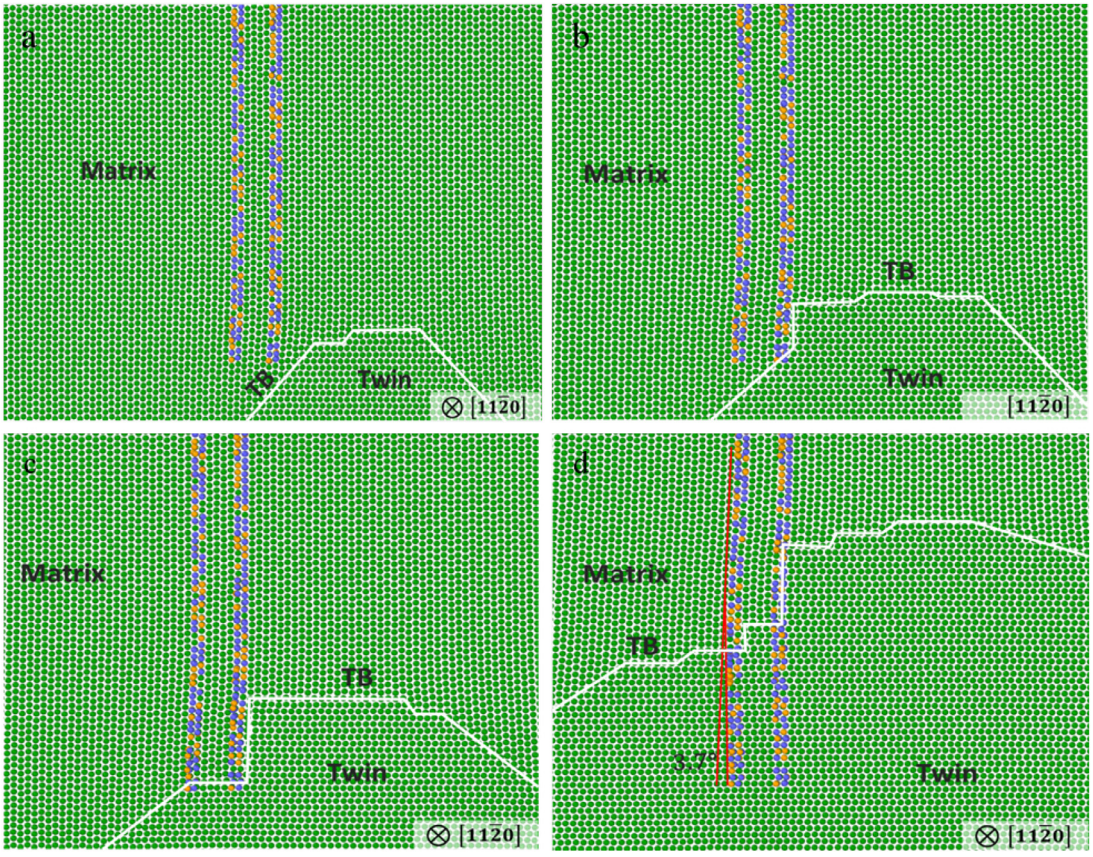

Fig. 7. MD simulations of structure transformation process from ∠86.3° QLPSO-twin structure to ∠3.7° QLPSO-twin structure (captured from Movie 2). (a-d) Typical time-lapse images of transformation process under different strains.

Please cite this article as: L. Zhou, T. Niu, G. Zou et al., High-strong-ductile magnesium alloys by interactions of nanoscale quasi-long period stacking order unit with twin, Journal of Magnesium and Alloys, https://doi.org/10.1016/j.jma.2024.01.015

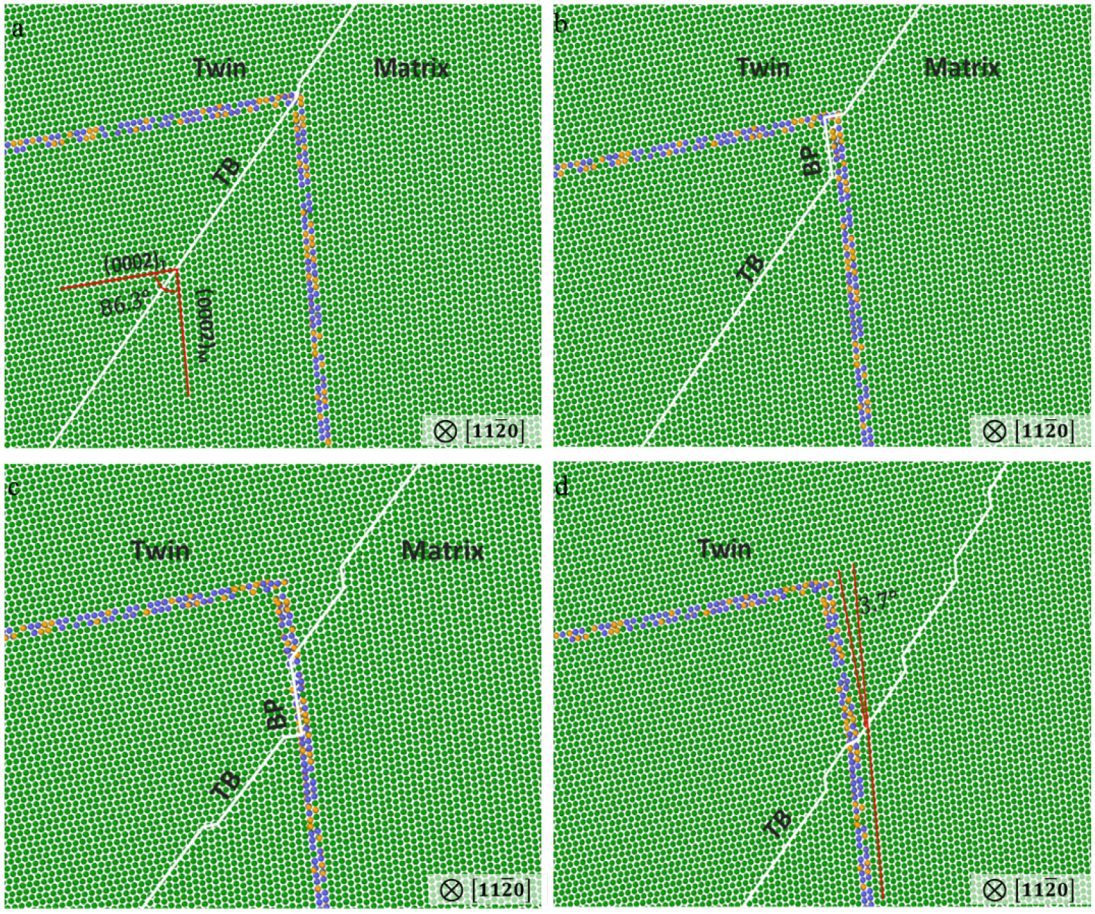

Fig. 8. MD simulations of the formation of ∠3.7° QLPSO-twin structure (captured from Movie 3). (a-d) Sequences of reaction process between QLPSO and twin.

structed following the TEM characterization by Tane et al [36]. As shown in Fig. 2g, the QLPSO structure presents co-segregation of Zn/Y atoms at basal stacking faults but without long-period stacking order. Thus, the QLPSO phases are constructed by randomly substituting solute atoms in the basal stacking fault layer. The corresponding nominal composition is approximately Mg-Zn4-Y6 (at. %), which is very close to LPSO phase [36].

Fig. 6 shows the interactions between TB and QLPSO with varying layers. For all cases, the TB initially remains stable as the stress increases. As the stress exceeds a critical value, the TB migration is initiated. Specifically, the critical yield stress is 0.62 GPa for the wide 18R LPSO phase. In stark contrast, the critical yield stresses of QLPSOs structure are merely about 67 % of the 18R LPSO phase owing to the thinner units. Note that the multiple-layered QLPSO structure has similar atomic layers as the 18R LPSO phase. Also noted from Supplementary Movie S1, the TB migration is strongly impeded in the presence of the 18R LPSO phase compared to QLPSOs. In addition, the interlayers of the 18R LPSO phase strongly drag the TB and form abundant BP interfaces (Fig. 6f).Therefore, the presence of large numbers of QLPSOs does not serve as a strong barrier for TB migration as compared to the LPSO phase. Thus, it is prone to motivate twinningin the UPed800-A300 Mg-0.2Zn-0.6Y alloy containing the nanosize QLPSO phases, resulting in the formation of hierarchical QLPSO-twin structure.

The formation of Mg alloys with LPSO structure is mainly associated with the kink deformation mode proposed by Orowan [37], wherein the kind band is a thin plate of sheared material in a crystal, transverse to a slip direction, bounded by opposite “tilt walls” of dislocations. So, LPSO lamellae can effectively inhibit the initiation and expansion of twins. The kinks in LPSO phase play a dominant role during the deformation process in Mg alloys with LPSO structure. This is also the reason for the high strength of Mg alloys containing LPSO phase but sacrificing its ductility. In contrast, the kink mode has hardly been detected in the UPed800-A300 Mg-0.2Zn-0.6Y alloy. On the contrary, there exist a large number of twins during the tension deformation process, as evidenced by TEM and STEM. This trend is similar to the reported results that the twins have occasionally been detected in the relatively thin LPSO lamellar [38]. Consequently, differing from the deformation (kinks) of Mg alloys with wide LPSO phase, twinning is the main deformation mode for Mg alloys with nanosize QLPSO structure.

Please cite this article as: L. Zhou, T. Niu, G. Zou et al., High-strong-ductile magnesium alloys by interactions of nanoscale quasi-long period stacking order unit with twin, Journal of Magnesium and Alloys, https://doi.org/10.1016/j.jma.2024.01.015

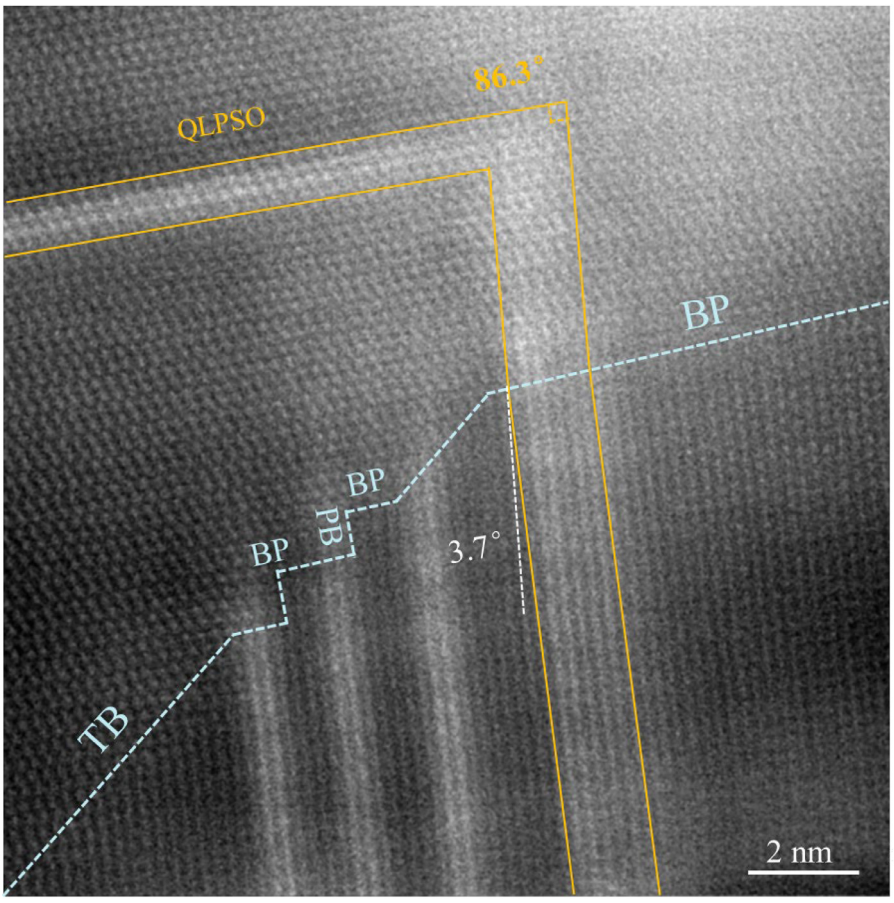

Fig. 9. Typical HRTEM image of ∠3.7° QLPSO-twin structure. It is formed by the structure transformation of ∠86.3° QLPSO-twin structure, which is consistent with the MD results.

4.2. QLPSO-twin interactive role

Two different QLPSO/TB interfaces (∠86.3° and ∠3.7°) are observed during the deformation process of the UPed800-A300 Mg-0.2Zn-0.6Y alloy. Moreover, the volume fraction of ∠3.7° QLPSO-twin interface is far higher than that of ∠86.3° QLPSO-twin interface. To elucidate the relationship of two interactive roles between QLPSO and twins, the reaction process has been clarified by MD simulations. In the mode I-TB free movement (Fig. 7 and Supplementary Movie S2), an isolated $\{10\bar{1}2\}$ TB firstly nucleates in the matrix, indicating the interior of QLPSO sites might have some prohibited role in the occurrence of twinning. Two distinct characters have been observed during this interactive process. On the one hand, as the stress increases TBs meet the QLPSO phase, and it directly cuts through double-layered QLPSOs. Moreover, the movement speed along QLPSOs is lower than that of the expanding rate in the matrix. On the other hand, the overall shape of QLPSO phase remains intact, but there is a new ∠3.7° deflection in the interface of QLPSO/TB, resulting in the formation of ∠3.7° QLPSO-twin interface. These typical structure characters are consistent with the above results identified by STEM (Fig. 5), in relative to the PB/BP transformation mechanism [39].

To further probe the relation of the two interface structures, we constructed a typical ∠86.3° QLPSO-twin interface. Specifically, a perfect tension twin with 86.3° was created firstly, and then two atomic layered QLPSO was inserted. A ∠86.3° QLPSO-twin structure has been built after relaxation (Fig. 8a). The TB migrates as the stress increases to a critical value. Initially, the TB movement near the intersection point of the ∠86.3° QLPSO is greatly delayed, leading to the formation of BP interface (Fig. 8b). However, as soon as the TB detaches the ∠86.3° QLPSO intersection point, the TB migrates along QLPSO (Fig. 8c-d), resulting in the formation of ∠3.7° QLPSO-twin structure due to the prismatic/basal transformation mechanism, i.e., the parent basal is transformed to twin prismatic. These structural characteristics (Supplementary Movie S3) have been well confirmed by HRTEM observation. As shown in Fig. 9, there are three typical characters in the TBs/QLPSO interface. Firstly, some high steps with four atomic layers are detected in the tip of QLPSO, revealing the QLPSO phase can, to some content, prohibit the TBs slide. Secondly, when the TBs slide away from the inflection point of QLPSO, it is prone to form ∠3.7° QLPSO-twin interface, which agrees well with the MD simulations. Thirdly, the continuous TBs structure maintains intact although it obviously deviates from the linear direction after

Please cite this article as: L. Zhou, T. Niu, G. Zou et al., High-strong-ductile magnesium alloys by interactions of nanoscale quasi-long period stacking order unit with twin, Journal of Magnesium and Alloys, https://doi.org/10.1016/j.jma.2024.01.015

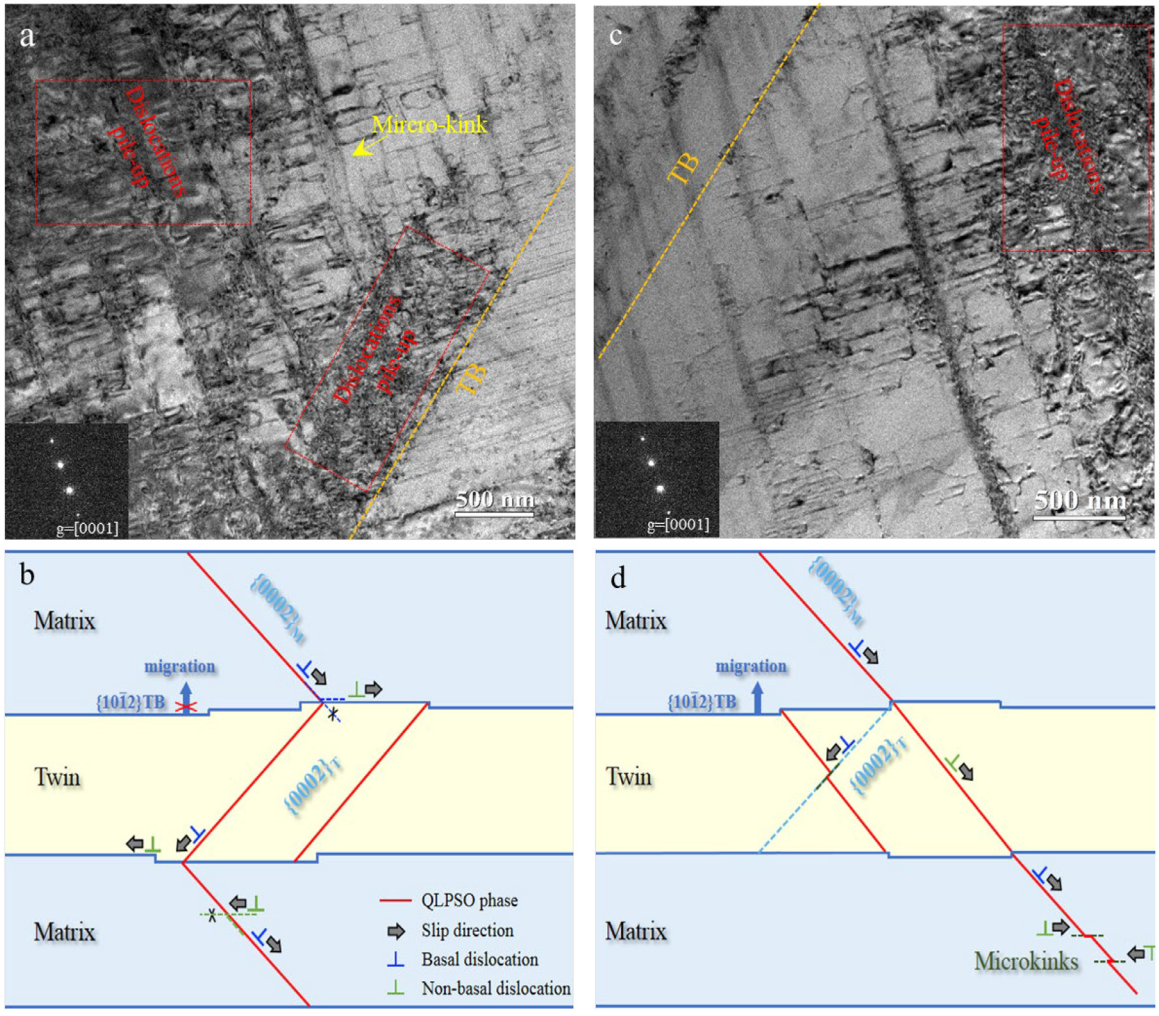

Fig. 10. Deformation behavior of different structures. (a) Bright-field image showing the high density dislocations were hindered by 86.3° QLPSO-twin structure and QLPSO phase, and the QLPSO phase adapts to strain in a kinked manner. (b) Schematic illustrations of strengthening mechanism of QLPSO-twin structure. (c) The dislocations are mainly hindered by the QLPSO phase. The ability of 3.7° QLPSO-twin structure to hinder dislocation movement significantly decreases. (d) Schematic illustrations of the ductile mechanism of QLPSO-twin structure.

multiple PB/BP transformations, which plays a crucial role in improving its mechanical properties.

4.3. Strong-ductile mechanism

The yield strength and elongation of UPed800-A300 Mg-0.2Zn-0.6Y sample is 205 MPa and 23 %, which is 2.41 and 1.54 times higher than those of single phase solid solution UPed800 Mg-0.2Zn-0.6Y alloy with a grain dimension of hundred micrometers (~55 MPa). Taking into account the similar grain size, the improved mechanical properties are mainly attributed to the formation of unique hierarchical QLPSO-twin structure. This interactive role has been further identified in the fractured UPed800-A300 Mg-0.2Zn-0.6Y sample. As indicated in Fig. 10a and c, a large number of dislocations accumulate along narrow QLPSO boundaries. Furthermore, a ∠86.3° QLPSO-twin interface becomes wide and vague owing to the pinning of dislocations, revealing that it also is effective to pin dislocation motion. At the same time, some micro-kinks with small misorientation angles (always less than 15°) are also observed after deformation, making the phase bend like a bowed caterpillar. Note that the ∠3.7° QLPSO-twin interface remains straight and flat, similar to the original morphology, suggesting it is weak to prohibit dislocation movement.

The strengthening mechanisms of UPed800-A300 Mg-0.2Zn-0.6Y sample are illustrated in Fig. 10b. Specifically, the main strengthening reasons stem from two aspects: (i) the QLPSO phases pin partial dislocations movement and (ii) the modified ∠86.3° TBs prohibit partial dislocations movement. Experimentally, these QLPSO-TBs interactions are similar in some way to hierarchical TB-TBs interactions dependent on dislocation pinning. The theoretical increased yield strength of pure QLPSO (similar to stacking faults) can be estimated by the following equation [40]:

$$\Delta\sigma = \mathrm{mkd}^{-1} \quad (4)$$

Where d is the average width of QLPSO (27.2 nm); m is the volume fraction, and k is experimental constant (3780 MPa nm). Therefore, the theoretical increase in yield strength of pure structure is 1.39 GPa.

Additionally, according to previous twin-twin strengthening mechanisms provided that the width of twin corresponds to the grain size, the theoretical increased yield strength of the unique QLPSO-twin can be estimated by the following equation [11,39]:

$$\Delta\sigma = m_1 k d^{-1} + m_2 k_t \lambda_1^{-1/2} \quad (5)$$

where λ_1 are the average widths of QLPSO and ∠86.3° twin, respectively; k_t is the Hall Petch constant (0.35 $MPam^{1/2}$), m_1 and m_2 are the volume fractions. Hence, the theoretical increment of yield strength of this unique QLPSO-twin structure is 2.15 GPa. Taking as m is 0.1, the increased value is about 215 MPa.

Two main reasons in unique QLPSO-twin structure attributes to enhanced ductility of UPed800-A300 Mg-0.2Zn-0.6Y sample, as shown in Fig. 10d. On the one hand, there is a large number fraction of ∠86.3° TBs in the deformation alloy. This interface is unstable, and it can easily slide along QLPSO phase. Moreover, it is prone to form high steps or bend in TBs. Both of them could release dislocations during the deformation process, resulting in high ductility. On the other hand, as the width of QLPSO is reduced, it is prone to form some micro-kinks instead of kinks (higher than 15°) (Fig. 9) during the plasticity deformation, which might be paved a possible way to improve its ductility.

5. Conclusion

In summary, ultrahigh pressure treatment provides an effective approach to modify the microstructure, phase composition and mechanical properties of the Mg-0.2Zn-0.6Y alloys. Some main conclusions can be drawn as follows:

1) A high volume-fraction of nano-sized QLPSO phases has firstly been achieved in the Mg-0.2Zn-0.6Y alloys after ultrahigh pressure treatment and annealing, wherein its width is about four-layer atoms and its average spacing is about 27.2 nm.
2) The UPed-T300 Mg-0.2Zn-0.6Y alloys containing the QLPSO structure show the maximum microhardness of 76±2 HV, near to twice higher than that of as-cast sample. More attractively, both high yield strength (205 MPa) and outstanding elongation (23 %) are simultaneously attained at room temperature, which exceeds the majority of the same alloying-level Mg alloys reported so far.
3) The $\{10\bar{1}2\}$ tension twin readily presents in the deformed UPed-T300 Mg-0.2Zn-0.6Y alloys containing the QLPSO structure, in which twin boundary is prone for form two interface interactive modes: ∠86.3° QLPSO-TB and ∠3.7° QLPSO-TB.
4) MD simulations exhibit that the formation of QLPSO-twin structure is related to the weak pinning role of thin QLPSO. Meanwhile, the ∠86.3°QLPSO-TB can be transferred into the ∠3.7° QLPSO-TB dependent of PB/BP transformation.
5) Dependent on both experimental and theoretical results, it is confirmed that the strengthening role is mainly associated with the presence of nanosized QLPSO and the modified ∠86.3° QLPSO-TB. In contrast, the enhanced ductility is attributed to the ∠3.7° QLPSO-TB and micro-kinks in QLPSO phases.

Declaration of competing interest

Qiuming Peng is an editorial board member for Journal of Magnesium and Alloys and was not involved in the editorial review or the decision to publish this article. All authors declare that there are no competing interests.

CRediT authorship contribution statement

Lutong Zhou: Project administration, Methodology, Investigation, Formal analysis, Data curation. **Tingting Niu:** Investigation. **Guodong Zou:** Supervision, Investigation. **Huhu Su:** Software, Formal analysis. **Suyun He:** Software, Formal analysis. **Shijian Zheng:** Resources. **Yulong Zhu:** Software, Resources, Data curation. **Peng Chen:** Software, Resources. **Carlos Fernandez:** Writing – review & editing. **Qiuming Peng:** Writing – review & editing, Writing – original draft.

Acknowledgements

We greatly acknowledge the financial support from National Natural Science Foundation of China (52171126, 51971194, 52202374 and 52331003), "S&T Program of Hebei" (236Z1020G) and the Natural Science Foundation of Hebei Province (E2022203167, E2023203255 and C2022203003). We would like to express our gratitude to Ministry of Education Yangtze River Scholar Professor Program (T2020124).

Supplementary materials

Supplementary material associated with this article can be found, in the online version, at doi:10.1016/j.jma.2024.01.015.

References

[1] Z. Wu, W.A. Curtin, Nature 526 (2015) 62–67.
[2] Y.M. Kim, C.D. Yim, B.S. You, Scr. Mater. 57 (2007) 691–694.
[3] A. Singh, M. Watanabe, A. Kato, A.P. Tsai, Scr. Mater. 51 (2004) 955–960.
[4] B. Ravaji, S.P. Joshi, Acta Mater. 208 (2021) 116743.
[5] L. Lu, X. Chen, K. Huang, Science 323 (2009) 607–610.
[6] Y. Tian, B. Xu, D. Yu, Y. Ma, Y. Wang, Y. Jiang, W. Hu, C. Tang, Y. Gao, K. Luo, Z. Zhao, L.-M. Wang, B. Wen, J. He, Z. Liu, Nature 493 (2013) 385–388.
[7] Y. Yue, Y. Gao, W. Hu, B. Xu, J. Wang, X. Zhang, Q. Zhang, Y. Wang, B. Ge, Z. Yang, Z. Li, P. Ying, X. Liu, D. Yu, B. Wei, Z. Wang, X.-F. Zhou, L. Guo, Y. Tian, Nature 582 (2020) 370–374.

[8] M. Lentz, M. Risse, N. Schaefer, W. Reimers, I.J. Beyerlein, Nat. Commun. 7 (2016) 11068.
[9] Y. Liu, N. Li, M. Arul Kumar, S. Pathak, J. Wang, R.J. McCabe, N.A. Mara, C.N. Tomé, Acta Mater. 135 (2017) 411–421.
[10] H. Fu, B. Ge, Y. Xin, R. Wu, C. Fernandez, J. Huang, Q. Peng, Nano Lett 17 (2017) 6117–6124.
[11] Q. Peng, Y. Sun, B. Ge, H. Fu, Q. Zu, X. Tang, J. Huang, Acta Mater. 169 (2019) 36–44.
[12] J.K. Kim, W.S. Ko, S. Sandlöbes, M. Heidelmann, B. Grabowski, D. Raabe, Acta Mater. 112 (2016) 171–183.
[13] M. Itakura, M. Yamaguchi, D. Egusa, E. Abe, Acta Mater. 203 (2021) 116491.
[14] S. Harjo, W. Gong, K. Aizawa, T. Kawasaki, M. Yamasaki, Acta Mater. 255 (2023) 119029.
[15] Y.J. Wu, X.Q. Zeng, D.L. Lin, L.M. Peng, W.J. Ding, J. Alloys. Compd. 477 (2009) 193–197.
[16] A.P. Thompson, H.M. Aktulga, R. Berger, D.S. Bolintineanu, W.M. Brown, P.S. Crozier, P.J. in't Veld, A. Kohlmeyer, S.G. Moore, T.D. Nguyen, R. Shan, M.J. Stevens, J. Tranchida, C. Trott, S.J. Plimpton, Comput. Phys. Commun. 271 (2022) 108171.
[17] M.I. Baskes, R.A. Johnson, Mater. Sci. Eng. 2 (1994) 147.
[18] H.S. Jang, K.M. Kim, B.J. Lee, Calphad 60 (2018) 200–207.
[19] K.H. Kim, J.B. Jeon, B.J. Lee, Calphad 48 (2015) 27–34.
[20] C.M. Baker, P.E.M. Lopes, X. Zhu, B.T. Roux, A.D. Mackerell, J. Chem. Theory Comput. 6 (2010) 1181.
[21] A.K. Rappe, C.J. Casewit, K.S. Colwell, W.A.I. Goddard, W.M.J. Skiff, J. UFF, Am. Chem. Soc. 114 (1992) 10024–10035.
[22] Q. Peng, W. Wu, J. Guo, J. Xiang, S.S. Zhao, J. Appl. Phys. 115 (2014) 2.
[23] J. Suh, J. Victoria-Hernández, D. Letzig, R. Golle, W. Volk, Mater. Sci. Eng. A. 669 (2016) 159–170.
[24] H. Miao, H. Huang, S. Fan, J. Tan, Z. Wang, W. Ding, G. Yuan, Mater Des. 196 (2020) 109122.
[25] C. Zhao, Z. Li, J. Shi, X. Chen, T. Tu, Z. Luo, R. Cheng, A. Atrens, F. Pan, J. Magnes. Alloys 7 (2019) 672–680.
[26] B.Q. Shi, R.S. Chen, W. Ke, Mater. Sci. Eng. A 560 (2013) 62–70.
[27] D.H. Lee, G.M. Lee, S.H. Park, J. Magnes. Alloys 11 (2023) 1683–1696.
[28] T. Nakata, T. Hama, K. Sugiya, S. Kamado, Mater. Sci. Eng. A 852 (2022) 143638.
[29] E.P. Silva, R.H. Buzolin, F. Marques, F. Soldera, U. Alfaro, H.C. Pinto, J. Magnes. Alloys 9 (2021) 995–1006.
[30] A. Orozco-Caballero, M. Álvarez-Leal, O.A. Ruano, F. Carreño, Mater. Sci. Eng. A 856 (2022) 143963.
[31] Y. Matsuoka, M. Bian, X. Huang, Y. Tsukada, T. Koyama, Y. Chino, J. Alloys Compd. 906 (2022) 164285.
[32] J.Y. Lee, Y.S. Yun, B.C. Suh, N.J. Kim, W.T. Kim, D.H. Kim, J. Alloys Compd. 589 (2014) 240–246.
[33] Y.M. Zhu, A.J. Morton, J.F. Nie, Acta Mater. 60 (2012) 6562–6572.
[34] Y. Yue, J.F. Nie, Scr. Mater. 218 (2022) 114842.
[35] S.Q. Zhu, S.P. Ringer, Acta Mater. 144 (2018) 365–375.
[36] M. Tane, H. Kimizuka, K. Hagihara, S. Suzuki, T. Mayama, T. Sekino, Y. Nagai, Acta Mater. 96 (2015) 170–188.
[37] E. Orowan, Nature 149 (1942) 643–644.
[38] F. Zhang, Y. Ren, Z. Yang, H. Su, Z. Lu, C. Tan, H. Peng, K. Watanabe, B. Li, M.R. Barnett, M. Chen, Acta Mater. 188 (2020) 203–214.
[39] Q. Zu, X.Z. Tang, S. Xu, Y.F. Guo, Acta Mater. 130 (2017) 310–318.
[40] S. Zhang, Y. Sun, R. Wu, X. Wang, X.B. Chen, C. Fernandez, Q. Peng, J. Mater. Sci. Technol. 51 (2020) 79–83.

Please cite this article as: L. Zhou, T. Niu, G. Zou et al., High-strong-ductile magnesium alloys by interactions of nanoscale quasi-long period stacking order unit with twin, Journal of Magnesium and Alloys, https://doi.org/10.1016/j.jma.2024.01.015